

Topological transport of vorticity on curved magnetic membranes

Chau Dao,¹ Ji Zou,² Eric Kleinherbers,¹ and Yaroslav Tserkovnyak¹

¹*Department of Physics and Astronomy and Bhaumik Institute for Theoretical Physics, University of California, Los Angeles, California 90095, USA*

²*Department of Physics, University of Basel, Klingelbergstrasse 82, CH-4056 Basel, Switzerland*

In this work, we study the transport of vorticity on curved dynamical two-dimensional magnetic membranes. We find that topological transport can be controlled by geometrically reducing symmetries, which enables processes that are not present in flat magnetic systems. To this end, we construct a vorticity 3-current which obeys a continuity equation. This continuity equation is immune to local fluctuations of the magnetic texture as well as spatiotemporal fluctuations of the membrane. We show how electric current can manipulate vortex transport in geometrically nontrivial magnetic systems. As an illustrative example, we propose a minimal setup that realizes an experimentally feasible energy storage device.

Introduction.—Much progress has been made both theoretically and experimentally in understanding, engineering, and driving topological magnetic textures [1–12]. This has resulted in numerous proposals that exploit spin texture topology for technological applications, such as domain wall and skyrmion racetracks [13–17], energy storage [18–20], long-range signal transport [21–29], and quantum information processing [30–32]. The utility of these spin structures is rooted in the metastability of topological excitations and the variety of ways to manipulate them [4, 11, 33–35]. To foster the development of these technologies, it is crucial to innovate avenues to drive topological textures. Motivated by the interplay between geometry and topology [36–38], we seek a way to geometrically control topological transport. Previous works have investigated geometrical effects in curved low-dimensional magnetic systems, primarily focusing on energetic stabilization of topological spin textures [39–44]. These developments are spurred by advancements in fabrication and imaging techniques for complex magnetic structures [43, 45–47].

In this letter, we study the transport of vorticity on curved magnetic membranes. To this end, we demonstrate that magnetic textures on membranes with curvature exhibit *topological hydrodynamics* [48] governed by a robust continuity equation rooted in the homotopic properties of the magnetic order parameter space, rather than any structural symmetries. In contrast to previous studies focused on vortex transport in flat magnetic films [20–22, 49], this work uses the spatial structure of magnetic systems to reduce symmetries, thereby enabling processes that are otherwise ruled out on symmetry grounds. We discuss how a nontrivial geometry can allow electric current to energetically bias vorticity injection on the membrane. Finally, we illustrate a potential functionality of this physics by devising an experimentally feasible energy storage concept.

Topological continuity equation.—We begin by discussing the geometric properties of a curved dynamical magnetic membrane. The membrane is a two-dimensional orientable manifold \mathcal{M} , parameterized by coordinates

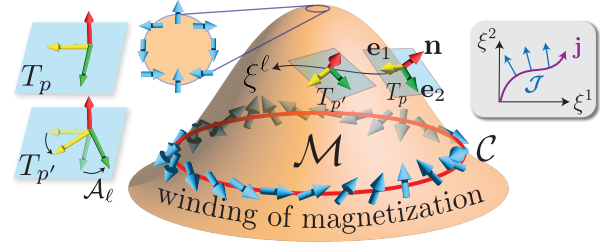


FIG. 1. Depiction of manifold \mathcal{M} . The winding of the magnetization \mathbf{m} (blue arrows) on the contour \mathcal{C} (red line) determines the vortex charge enclosed by \mathcal{C} . The local tangent planes T_p and $T_{p'}$ are shown for points p and p' , along with the local frame $\{\mathbf{e}_1, \mathbf{e}_2, \mathbf{n}\}$. The leftmost tangent planes depict the gauge potential \mathcal{A}_ℓ at point p' , which captures changes of \mathbf{e}_1 and \mathbf{e}_2 along ξ^ℓ . The inset shows vorticity flux \mathcal{J} being pumped transverse to a metallic wire (purple curve) carrying electric current density \mathbf{j} .

ξ^1 and ξ^2 , with boundary $\partial\mathcal{M}$. \mathcal{M} is embedded in the Euclidean space \mathbb{R}^3 from which it inherits the metric g_{ij} . At every point (ξ^1, ξ^2) on \mathcal{M} and for any time t , we identify a unit normal vector $\mathbf{n}(t, \xi^1, \xi^2)$ and define unit vectors spanning the local tangent plane, $\mathbf{e}_1(t, \xi^1, \xi^2)$ and $\mathbf{e}_2(t, \xi^1, \xi^2)$. The orthonormal triad $\{\mathbf{e}_1, \mathbf{e}_2, \mathbf{n}\}$ is the local frame. \mathcal{M} may smoothly change over time, as long as its topology remains unchanged, i.e. \mathcal{M} is not cut. Figure 1 depicts the simplest case in which \mathcal{M} is homeomorphic to a closed disk.

The $U(1)$ gauge freedom in specifying the local frame, corresponding to simultaneous rotations of \mathbf{e}_1 and \mathbf{e}_2 about \mathbf{n} , translates into the gauge potential [50–52]

$$\mathcal{A}_\mu = \mathbf{e}_1 \cdot \partial_\mu \mathbf{e}_2, \quad (1)$$

which is a smooth field describing changes of the local frame in space and time. Once the \mathbf{e}_1 and \mathbf{e}_2 vector fields are specified, the gauge is fixed. The spatial component of the gauge, \mathcal{A}_i , is the smooth connection on \mathcal{M} , which captures changes in \mathbf{e}_1 and \mathbf{e}_2 along ξ^i [51]. The gauge-invariant field strength tensor stemming from \mathcal{A}_μ is

$$\mathcal{F}_{\mu\nu} = \partial_\mu \mathcal{A}_\nu - \partial_\nu \mathcal{A}_\mu. \quad (2)$$

The “electric” component, \mathcal{F}_{0i} , vanishes for static membranes. The “magnetic” component, \mathcal{F}_{ij} , relates to the Gaussian curvature \mathcal{K} by $\mathcal{K} = \epsilon^{0ij}\mathcal{F}_{ij}/2\sqrt{g}$. Here, g is the determinant of the metric and the Levi-Civita tensor convention is $\epsilon^{012} = 1$. Note, we make a convention in which Greek indices $\mu = 0, 1, 2 \leftrightarrow t, \xi^1, \xi^2$ label space-time coordinates and Latin indices $i = 1, 2 \leftrightarrow \xi^1, \xi^2$ label spatial coordinates, while repeated indices are summed over.

We assume the magnetic texture is described by a continuum coarse-grained vector field $\mathbf{m}(t, \xi^1, \xi^2)$ realizing the map $\mathcal{M} \mapsto \mathbb{R}^3$ at all times t . This description holds over a broad temperature range, from order to disorder. In the low-temperature (locally) ordered phase, \mathbf{m} is normalized by its $T = 0$ value and the membrane can be either ferromagnetic or antiferromagnetic. \mathbf{m} is the local spin density in the former case, whereas in the latter case, \mathbf{m} is the local Néel order. In the high-temperature paramagnetic regime, \mathbf{m} may fluctuate in both magnitude and direction. Irrespective of any local fluctuations of \mathbf{m} or dynamics of \mathcal{M} , the field \mathbf{m} exhibits topological hydrodynamics governed by the continuity equation $\partial_\mu \mathcal{J}^\mu = 0$, where

$$\mathcal{J}^\mu = \frac{\epsilon^{\mu\nu\rho}}{2\pi} \left[\mathbf{n} \cdot (\nabla_\nu \mathbf{m} \times \nabla_\rho \mathbf{m}) - \frac{1}{2} \mathcal{F}_{\nu\rho} \mathbf{m}_\parallel^2 \right], \quad (3)$$

written using the covariant derivative of \mathbf{m}

$$\nabla_\mu \mathbf{m} \equiv (\partial_\mu m^a) \mathbf{e}_a - \mathcal{A}_\mu (\mathbf{n} \times \mathbf{m}), \quad (4)$$

which is gauge-invariant. Here, \mathbf{m}_\parallel is the projection of \mathbf{m} onto the local tangent plane. $\mathcal{J}^\mu = (\mathcal{J}^0, \mathcal{J})$ is the vorticity 3-current, where \mathcal{J}^0 is the vorticity density and \mathcal{J} is the vorticity flux. Furthermore, \mathcal{J}^μ is gauge-invariant under “small” gauge transformations which preserve the smoothness of \mathcal{A}_μ so that the covariant derivative is well-defined [50, 53, 54]. In the absence of curvature and membrane dynamics, the frame can be made constant and the vorticity 3-current reduces to $\mathcal{J}^\mu = \epsilon^{\mu\nu\rho} \mathbf{n} \cdot (\partial_\nu \mathbf{m} \times \partial_\rho \mathbf{m})/2\pi$ [20, 22].

The continuity equation is rooted in topology and is not derived from Noether’s theorem, so it is immune to any structural imperfections or anisotropies. The behavior of the system, on the other hand, will be highly sensitive to these details [3, 55]. In this work, we will focus on systems in which magnetic vorticity may be the natural transport quantity. We consider magnetic membranes with easy-surface anisotropy, i.e. there is a hard anisotropy axis collinear with the surface normal [41, 56], that endows the magnetic texture with an XY character [3, 57].

Gauge-invariant topological charge.—To construct the gauge-invariant vortex charge, the starting point is to construct the magnetic winding. For flat magnetic films, it is known that the winding along a curve is $\mathbf{m}_\parallel^2 \partial_\ell \varphi / 2\pi$ [20, 22, 27], with ℓ the arclength. Following this structure, the winding on curved membranes generalizes to the covariant

winding $\mathbf{m}_\parallel^2 D_i \varphi / 2\pi \equiv \mathbf{m}_\parallel^2 (\partial_i \varphi - \mathcal{A}_i) / 2\pi$, which is gauge-invariant. Here, φ is the polar in-(tangent)-plane angle of \mathbf{m}_\parallel relative to \mathbf{e}_1 . For φ to be well-defined, we require $|\mathbf{m}_\parallel| > 0$ everywhere on \mathcal{M} , except for isolated points. Invoking the generalized Stokes’ theorem [36, 58], the gauge-invariant topological charge on a patch \mathcal{S} is

$$\mathcal{Q} = \frac{1}{2\pi} \int_{\partial\mathcal{S}} d\xi^i \mathbf{m}_\parallel^2 D_i \varphi = \int_{\mathcal{S}} d\xi^1 d\xi^2 \mathcal{J}^0. \quad (5)$$

We see that the integrated winding around the boundary $\partial\mathcal{S}$ equals the vorticity density integrated over \mathcal{S} . In fact, we construct the conserved density \mathcal{J}^0 by taking the exterior derivative of the winding 1-form in the leftmost integral. We articulate this construction later in the text and in the Supplemental Material [59].

Even when specializing to the strong easy-surface limit where $|\mathbf{m}_\parallel| = 1$, \mathcal{Q} is noninteger-valued if \mathcal{M} has nonzero Gaussian curvature. In this limit, \mathcal{Q} can be evaluated for a patch \mathcal{S} homeomorphic to a disk (upon choosing a smooth gauge) to be $\mathcal{N} - \int_{\mathcal{S}} dS \mathcal{K} / 2\pi$. This is the difference of an integer \mathcal{N} which counts the number of vortices on \mathcal{S} and a geometric background offset that spoils the discreteness of \mathcal{Q} . \mathcal{N} is the S^1 winding number connecting \mathcal{Q} to its homotopic roots.

Torsion-enabled pumping of vorticity.—Having established a conserved topological charge, we now wish to control it. Suppose we wrap a magnetic membrane with a metallic wire parameterized by unit tangent vector $\mathbf{v}(\ell)$, with ℓ the arclength, and induce electric current flow in the wire. Following the approach developed in Refs. [20, 22], we construct a torque acting on a smooth magnetic texture, which energetically biases vorticity injection transverse to the wire, as depicted in the inset of Fig. 1. To enable this process, we use the local torsion of the wire, $\mathfrak{T}(\ell) = \mathbf{v} \cdot (\mathbf{a} \times \partial_\ell \mathbf{a})$, to geometrically reduce symmetries [58]. The torsion is the helical winding of the principal normal vector $\mathbf{a}(\ell) = \partial_\ell \mathbf{v} / |\partial_\ell \mathbf{v}|$ along the wire. Notably, torsion is a pseudoscalar, meaning $\mathfrak{T}\mathbf{n}$ is a pseudovector with identical spatial properties to magnetization. In this scheme, the role $\mathfrak{T}\mathbf{n}$ plays in reducing symmetries is analogous to that of magnetization \mathbf{M} in Refs. [20, 22].

The torque, which must be gauge-invariant, is constructed on general symmetry grounds so that the work done on the magnetic texture is proportional to the vorticity flow across the wire. Focusing, for simplicity, on the low-temperature limit where $|\mathbf{m}| = 1$, a torque (per unit length) satisfying these constraints is

$$\boldsymbol{\tau} = \frac{\zeta j}{\pi} (\mathfrak{T}\mathbf{n} \cdot \mathbf{m}) [\nabla_\ell \mathbf{m} + \mathbf{n} \partial_\ell (\mathbf{n} \cdot \mathbf{m})]. \quad (6)$$

Here, j is the electric current density, and ζ is a phenomenological parameter characterizing the geometry-enabled dissipative coupling of electric and vortex dynamics. Importantly, this torque is only permitted in the presence of spin-orbit coupling. This reminds us of the

chirality-induced spin selectivity effect, which arises from the coupling of the electron linear momentum to spin degrees of freedom in chiral materials [60, 61]. Furthermore, in the limit of strong spin-orbit coupling, dimensional analysis suggests $\zeta \sim \hbar w \lambda_F^2 / e$, where λ_F is the Fermi wavelength, e is the positive elementary electric charge, and w is the width of the wire. We assume $w \gg \lambda_F$ and that w is small enough for τ to be (approximately) uniform over the wire width.

The work done on the magnetic texture is

$$\delta W = \int dl dt \boldsymbol{\tau} \cdot (\mathbf{m} \times \partial_t \mathbf{m}) = \zeta \boldsymbol{\mathfrak{T}} j \delta Q, \quad (7)$$

where $\delta Q = \int dt dl \mathbf{v} \cdot (\boldsymbol{\mathcal{J}} \times \mathbf{n})$ is the vorticity flow across the wire. The effective vortex chemical potential is given by $\mu \equiv \delta W / \delta Q = \zeta \boldsymbol{\mathfrak{T}} j$. In the high-temperature paramagnetic regime, a linear relation $\mu \propto j$ should still hold, albeit with a prefactor renormalized by thermal fluctuations of $|\mathbf{m}|$.

Vortex circuit elements.—Fig. 2 illustrates a possible setup in which torsion gives rise to pumping of vorticity. Here, a magnetic insulating membrane (which can either be ferro- or antiferromagnetic) of thickness h and length l_m wraps around a cylindrical insulating core. A metal wire of width w and thickness δ is wrapped around the cylindrical magnetic membrane of radius r as a uniform helix with helix angle θ . Systems with similar geometry, in the form of rolled magnetic membranes, have been fabricated [62]. The uniform helix has a constant torsion $\boldsymbol{\mathfrak{T}} = \sin(2\theta)/2r$, allowing electric current flow in the wire to drive a vorticity flux $\boldsymbol{\mathcal{J}}$, which we assume is transverse to the wire.

$\boldsymbol{\mathcal{J}}$ can be decomposed into components orthogonal and parallel to the z axis. The former accumulates winding along z , which may unwind at the ends of the cylinder. The latter, on the other hand, builds up winding azimuthally, which is energetically protected by the easy-surface anisotropy. We are interested in the vortex current flowing in the z direction, $I_v = 2\pi r |\boldsymbol{\mathcal{J}}| \sin \theta$, which is driven by the vortex motive force $I \boldsymbol{\mathfrak{R}}$ generated by the electric current. Here,

$$\boldsymbol{\mathfrak{R}} = \frac{\zeta \boldsymbol{\mathfrak{T}} l_m}{2\pi r w \delta} \tan \theta \quad (8)$$

is the effective drag coefficient [59]. Different from our previous works on energy storage using topological spin textures [19, 20], $\boldsymbol{\mathfrak{R}}$ is unique to the nontrivial geometry of this setup and is not present in flat systems. Upon substitution of $\boldsymbol{\mathfrak{T}} = \sin(2\theta)/2r$, we find $\boldsymbol{\mathfrak{R}} \propto \sin^2 \theta$. In the linear response, $I_v \propto \boldsymbol{\mathfrak{R}}$, so $\theta = \pi/2$ maximizes the vortex current.

The membrane behaves like a series $R_v C_v$ circuit in response to nonzero vortex flow, exhibiting an effective vortex resistance R_v and effective winding capacitance C_v . As dictated by the bulk-boundary correspondence, the

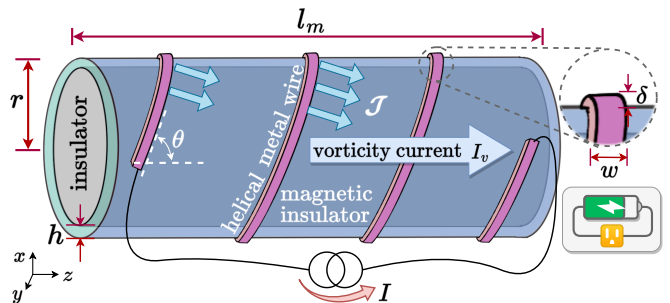


FIG. 2. Schematic of a minimal setup for geometrically controlled vortex transport. A metallic wire is wrapped around a cylindrical magnetic insulator membrane as a helix. An applied electric current I induces vorticity flux $\boldsymbol{\mathcal{J}}$ transverse to the wire, resulting in vorticity current I_v along z . The side panel indicates that this system realizes a battery.

vortex current “winds up” the magnetic texture, thereby storing exchange energy. The stiffness of the magnetic texture engenders C_v . On the other hand, R_v can arise due to Gilbert damping, defects, and vortex-antivortex collisions. Following Ref. [20], we estimate C_v and R_v by exploiting the duality between the XY magnet and two-dimensional electrostatics [57]. This yields

$$C_v = \frac{1}{A} \frac{r}{2\pi h l_m}, \quad R_v = \frac{1}{\sigma_v} \frac{l_m}{2\pi r}, \quad (9)$$

where σ_v^{-1} is the vortex resistivity and A is the magnetic stiffness [59]. With the circuit elements $\boldsymbol{\mathfrak{R}}$, R_v , and C_v in hand, we set out to construct topological circuits [20].

Coupled topological circuits.—The setup we have been discussing can be described by coupled vorticity and electric circuits, which are depicted in Fig. 3. The applied electric current I in the wire supplies an effective vortex motive force $I \boldsymbol{\mathfrak{R}}$ to the vorticity circuit. This results in build-up of winding and an effective vortex voltage $V_v = -Q/C_v$. The backaction of vortex dynamics on the electrical response induces an electromotive force $I_v \boldsymbol{\mathfrak{R}}$ on the electric circuit, which is written down by invoking Onsager reciprocity. We note that, like ordinary charge, vorticity is even under time reversal. Kirchhoff’s law for the coupled electrical and vorticity circuits is thus

$$\begin{pmatrix} V \\ V_v \end{pmatrix} = \begin{pmatrix} R + L \frac{d}{dt} & -\boldsymbol{\mathfrak{R}} \\ -\boldsymbol{\mathfrak{R}} & R_v \end{pmatrix} \begin{pmatrix} I \\ I_v \end{pmatrix}. \quad (10)$$

Here, V is the voltage supplying the current I , L is the self-inductance, and R is the electrical resistance. The resistance matrix is symmetric as dictated by Onsager reciprocity, and positive-definite according to the second law of thermodynamics [63, 64]. The latter constraint enforces $0 < \xi < 1$, where $\xi \equiv \boldsymbol{\mathfrak{R}}^2 / R R_v$ parameterizes the relative strength of the off-diagonal to the diagonal elements of the resistance matrix.

Fourier transforming Eq. (10) into the frequency do-

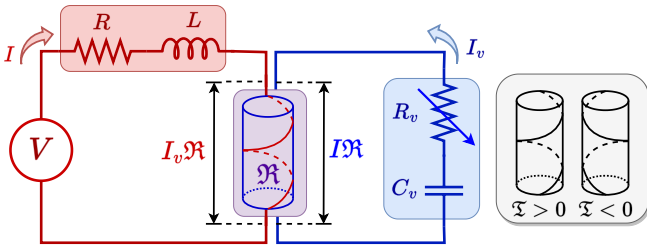


FIG. 3. Schematic of the vorticity (blue) and electric (red) circuits, which are coupled through \mathfrak{R} (purple). \mathfrak{R} gives rise to an effective vortex motive force $I\mathfrak{R}$ on the vorticity circuit and, reciprocally, an electromotive force $I_v\mathfrak{R}$ on the electrical response. R_v is tunable, allowing switching between vortex conducting and insulating regimes. The side panel depicts setups with positive and negative \mathfrak{T} .

main, we find the effective impedance is

$$Z(\omega) \equiv \frac{V(\omega)}{I(\omega)} = R + i\omega L - \frac{i\omega C_v \mathfrak{R}^2}{1 + i\omega C_v R_v}. \quad (11)$$

Similar to conventional RC circuits, here, $\tau = R_v C_v = (4\pi^2 A h \sigma_v)^{-1}$ is the time scale for loading and discharging vortices from the magnetic texture. In the high-frequency regime, $\omega \gg 1/\tau$, the last term in Eq. (11) is approximated as $-\mathfrak{R}^2/R_v$. The vorticity circuit functions as a battery, reducing the effective resistance of the electrical circuit. In the low-frequency limit, $\omega \ll 1/\tau$, the vorticity circuit acts like an inductor with effective negative inductance $L_v = -C_v \mathfrak{R}^2$. Impedance measurements of the circuit in the low-frequency regime could pave a way to probe the strength of the coupling between vortex and charge currents. Similar impedance measurements on helical-spin magnets have been performed to characterize the current-driven dynamics of spin-helix structures [65].

Energy storage and efficiency.—In addition to providing a means to measure ζ , the setup depicted in Fig. 2 may also function as a battery. Operation of the battery requires a mechanism to switch the vortex conductivity between the conducting and insulating regimes, allowing the battery to alternate between (dis)charging and storing energy, respectively. The vortex transport parameters could be very sensitive and may be modulated, for example, by heating and cooling the magnet [20, 57].

To charge the battery, we electrically bias vortex flow along z , building up azimuthal spin winding so the magnet accumulates exchange energy. Discharging the battery is the reverse process wherein a vortex current induces an electromotive force on the electric circuit, which may be extracted as energy. The exchange energy is stored by lowering the vortex conductivity, so vortex transport parameters enter the insulating regime. Once in the insulating regime, the amount of winding we can stabilize is governed by the Landau criterion, since the magnetic bulk cannot host an arbitrarily sharp texture [19, 66]. The easy-surface anisotropy ($\sim K$) protects the topologi-

cal spin texture by energetically preventing “phase-slip” events during which the magnetic order parameter unwinds [67]. Thus, easy-surface anisotropy determines the maximal energy storage capacity, which is saturated when winding texture energy [$\sim A(D_\ell \varphi)^2$] is comparable to K .

The charging and discharging efficiencies may be used to characterize the battery. In the vortex conducting regime, we charge the battery relative to its ground state by supplying a dc electric current I_0 for duration τ . By tuning R_v , we can switch to the vortex insulating regime to store the energy in the winding capacitor. The charging efficiency η_c is the ratio of the stored energy to the total energy supplied by the electric circuit. We extract the stored energy by connecting the battery to a load resistor R_L , then switching back to the vortex conducting regime to discharge. The discharging efficiency η_d is the ratio of energy consumed by R_L to the energy leaving the winding capacitor.

Neglecting the self-inductance L , the efficiencies are

$$\eta_c = \frac{1}{2} \frac{(1 - e^{-1})^2}{\mathcal{Z}_v^{-1} + e^{-1}}, \quad \eta_d = \frac{1 - \gamma}{1 + (\mathcal{Z}_v \gamma)^{-1}}, \quad (12)$$

written with $\gamma = R_L/(R_L + R)$ and $\mathcal{Z}_v \equiv \xi/(1 - \xi)$, where $\xi = \mathfrak{R}^2/RR_v$. Here, we define the charge-vortex figure of merit \mathcal{Z}_v by analogy to the thermoelectric figure of merit ZT [68–70]. Whereas for the thermoelectric effect, heat and charge currents are coupled, in this setting, we cross-couple vortex and electric currents. Since \mathcal{Z}_v is a monotonic function of ξ , optimizing the system geometry to maximize $\xi \sim adw\lambda_F^2 \sin^4 \theta \cos \theta / hr^3 \delta$ maximizes \mathcal{Z}_v and, hence, the efficiencies. Here, d is the electron mean free path and a is the lattice spacing. \mathcal{Z}_v is improved by decreasing r , thinning the membrane and the metal wire by decreasing δ and h , or enlarging the metal-magnet interface by increasing w . The optimal helix angle is $\theta \approx 63^\circ$, which balances maximizing I_v and minimizing energy lost due to Joule heating. In the maximal efficiency limit, $\mathcal{Z}_v \rightarrow \infty$, the efficiencies simplify to $\eta_c = (e - 1)^2/2e$ and $\eta_d = 1 - \gamma$ for (dis)charging times of $t = \tau$. Furthermore, in the short charging time limit of $t/\tau \rightarrow 0$, while still having $\mathcal{Z}_v \rightarrow \infty$, the charging efficiency saturates as $\eta_c \rightarrow 1$.

Higher-dimensional generalization.—Topological hydrodynamics may be formulated using differential forms for static manifolds and is extendable to higher dimensions. For an n -dimensional orientable manifold, the integral of an $(n - 1)$ -form $\tilde{\rho}_w$ over the $(n - 1)$ -dimensional boundary of a patch of the manifold is conserved. The density n -form $\tilde{\rho}_v$ and the flux 1-form \tilde{j}_v are derived from $\tilde{\rho}_w$ by invoking Stokes’ theorem. We define $\tilde{\rho}_v$ as the exterior derivative of $\tilde{\rho}_w$, yielding $\tilde{\rho}_v = d\tilde{\rho}_w$. Applying the Hodge star map [36, 58] and taking the time derivative of both sides, $\tilde{\rho}_v = d\tilde{\rho}_w$ is recast as the continuity equation $\star \partial_t \tilde{\rho}_v + \star d \star \tilde{j}_v = 0$, where $\tilde{j}_v = (-1)^n \star \partial_t \tilde{\rho}_w$. Returning to the 2-dimensional membrane, \mathcal{Q} in Eq. (5) is written

using the winding 1-form ρ_w as

$$Q = \int_{\partial\mathcal{M}} \rho_w = \frac{1}{2\pi} \int_{\partial\mathcal{M}} d\xi^i \mathbf{n} \cdot (\mathbf{m} \times \nabla_i \mathbf{m}). \quad (13)$$

The vorticity density 2-form ρ_v and the vorticity flux 1-form j_v stem from ρ_w and are written in terms of \mathcal{J}^μ from Eq. (3) as $\rho_v = d\xi^1 d\xi^2 \mathcal{J}^0$ and $j_v = d\xi^i g_{ij} \mathcal{J}^j / \sqrt{g}$. They satisfy $\star \partial_t \rho_v + \star d \star j_v = 0$, which is equivalent to $\partial_\mu \mathcal{J}^\mu = 0$.

Discussion.—In this work, we developed topological hydrodynamics for vortices on curved membranes and devised a means to geometrically control vortex transport. To achieve this, we constructed the vorticity 3-current and phenomenologically introduced a torque that uses geometric torsion to enable electric current-induced vortex pumping. With these building blocks, we analyzed a minimal setup which is described by an effective coupled electrical-vorticity circuit and realizes a feasible energy storage concept.

For future works, it would be intriguing to extend our formalism to manifolds with different topologies. These setups may potentially be achieved by modern fabrication techniques, which have been employed to manufacture complex magnetic structures [44, 62, 71, 72]. Another possible direction would be to expand beyond vortex circuit elements and develop logic elements based on this physics.

Acknowledgments. We thank Denys Sheka and Se Kwon Kim for insightful discussions. This work was primarily supported by the U.S. Department of Energy, Office of Basic Energy Sciences under Grant No. DE-SC0012190. J.Z. acknowledges the support of the Georg H. Endress Foundation.

-
- [1] J. Zang, V. Cros, and A. Hoffmann, *Topology in magnetism*, Vol. 192 (Springer, 2018).
- [2] S. Maekawa, S. O. Valenzuela, E. Saitoh, and T. Kimura, *Spin current*, Vol. 22 (Oxford University Press, 2017).
- [3] A. M. Turner, V. Vitelli, and D. R. Nelson, Vortices on curved surfaces, *Rev. Mod. Phys.* **82**, 1301 (2010).
- [4] X. Zhang, Y. Zhou, K. M. Song, T.-E. Park, J. Xia, M. Ezawa, X. Liu, W. Zhao, G. Zhao, and S. Woo, Skyrmion-electronics: writing, deleting, reading and processing magnetic skyrmions toward spintronic applications, *J. Phys. Condens. Matter* **32**, 143001 (2020).
- [5] K. Mæland and A. Sudbø, Topological superconductivity mediated by skyrmionic magnons, *Phys. Rev. Lett.* **130**, 156002 (2023).
- [6] S. S. Cherepov, B. C. Koop, A. Y. Galkin, R. S. Khymyn, B. A. Ivanov, D. C. Worledge, and V. Korenivski, Core-core dynamics in spin vortex pairs, *Phys. Rev. Lett.* **109**, 097204 (2012).
- [7] X.-G. Wang, G.-h. Guo, A. Dyrdał, J. Barnaś, V. K. Dugaev, S. S. P. Parkin, A. Ernst, and L. Chotorlishvili, Skyrmion echo in a system of interacting skyrmions, *Phys. Rev. Lett.* **129**, 126101 (2022).
- [8] S. Dasgupta, S. Zhang, I. Bah, and O. Tchernyshyov, Quantum statistics of vortices from a dual theory of the *xy* ferromagnet, *Phys. Rev. Lett.* **124**, 157203 (2020).
- [9] A. Rana, C.-T. Liao, E. Iacocca, J. Zou, M. Pham, X. Lu, E.-E. C. Subramanian, Y. H. Lo, S. A. Ryan, C. S. Bevis, R. M. Karl, A. J. Glaid, J. Rable, P. Mahale, J. Hirst, T. Ostler, W. Liu, C. M. O’Leary, Y.-S. Yu, K. Bustillo, H. Ohldag, D. A. Shapiro, S. Yazdi, T. E. Mallouk, S. J. Osher, H. C. Kapteyn, V. H. Crespi, J. V. Badding, Y. Tserkovnyak, M. M. Murnane, and J. Miao, Three-dimensional topological magnetic monopoles and their interactions in a ferromagnetic meta-lattice, *Nat. Nanotechnol.* **18**, 227 (2023).
- [10] E. Schwartz, B. Li, and A. A. Kovalev, Superfluid spin transistor, *Phys. Rev. Res.* **4**, 023236 (2022).
- [11] M. Vogel, B. Zimmermann, J. Wild, F. Schwarzhuber, C. Mewes, T. Mewes, J. Zweck, and C. H. Back, Driving a magnetic texture by magnon currents, *Phys. Rev. B* **107**, L100409 (2023).
- [12] M. Stepanova, J. Masell, E. Lysne, P. Schoenherr, L. Köhler, M. Paulsen, A. Qaiumzadeh, N. Kanazawa, A. Rosch, Y. Tokura, A. Brataas, M. Garst, and D. Meier, Detection of topological spin textures via nonlinear magnetic responses, *Nano Lett.* **22**, 14 (2022).
- [13] S. S. P. Parkin, M. Hayashi, and L. Thomas, Magnetic domain-wall racetrack memory, *Science* **320**, 190 (2008).
- [14] R. Bläsing, A. A. Khan, P. C. Filippou, C. Garg, F. Hameed, J. Castrillon, and S. S. P. Parkin, Magnetic racetrack memory: From physics to the cusp of applications within a decade, *Proc. IEEE* **108**, 1303 (2020).
- [15] R. Tomasello, E. Martinez, R. Zivieri, L. Torres, M. Carpentieri, and G. Finocchio, A strategy for the design of skyrmion racetrack memories, *Sci. Rep.* **4**, 1 (2014).
- [16] R. Tomasello, V. Puliafito, E. Martinez, A. Manchon, M. Ricci, M. Carpentieri, and G. Finocchio, Performance of synthetic antiferromagnetic racetrack memory: domain wall versus skyrmion, *J. Phys. D* **50**, 325302 (2017).
- [17] J. Müller, Magnetic skyrmions on a two-lane racetrack, *New J. Phys.* **19**, 025002 (2017).
- [18] R. M. Otxoa, R. Rama-Eiroa, P. E. Roy, G. Tatara, O. Chubykalo-Fesenko, and U. Atxitia, Topologically-mediated energy release by relativistic antiferromagnetic solitons, *Phys. Rev. Res.* **3**, 043069 (2021).
- [19] Y. Tserkovnyak and J. Xiao, Energy storage via topological spin textures, *Phys. Rev. Lett.* **121**, 127701 (2018).
- [20] D. Jones, J. Zou, S. Zhang, and Y. Tserkovnyak, Energy storage in magnetic textures driven by vorticity flow, *Phys. Rev. B* **102**, 140411 (2020).
- [21] J. Zou, S. Zhang, and Y. Tserkovnyak, Topological transport of deconfined hedgehogs in magnets, *Phys. Rev. Lett.* **125**, 267201 (2020).
- [22] J. Zou, S. K. Kim, and Y. Tserkovnyak, Topological transport of vorticity in heisenberg magnets, *Phys. Rev. B* **99**, 180402(R) (2019).
- [23] L. Cornelissen, J. Liu, R. Duine, J. B. Youssef, and B. Van Wees, Long-distance transport of magnon spin information in a magnetic insulator at room temperature, *Nat. Phys.* **11**, 1022 (2015).
- [24] X. Wang, A. Qaiumzadeh, and A. Brataas, Current-driven dynamics of magnetic hopfions, *Phys. Rev. Lett.* **123**, 147203 (2019).
- [25] D. Raftrey and P. Fischer, Field-driven dynamics of magnetic hopfions, *Phys. Rev. Lett.* **127**, 257201 (2021).
- [26] Y. Liu, W. Hou, X. Han, and J. Zang, Three-dimensional

- dynamics of a magnetic hopfion driven by spin transfer torque, *Phys. Rev. Lett.* **124**, 127204 (2020).
- [27] Y. Tserkovnyak, J. Zou, S. K. Kim, and S. Takei, Quantum hydrodynamics of spin winding, *Phys. Rev. B* **102**, 224433 (2020).
- [28] Y. Tserkovnyak and J. Zou, Quantum hydrodynamics of vorticity, *Phys. Rev. Res.* **1**, 033071 (2019).
- [29] S. Zhang and Y. Tserkovnyak, Antiferromagnet-based neuromorphics using dynamics of topological charges, *Phys. Rev. Lett.* **125**, 207202 (2020).
- [30] C. Psaroudaki and C. Panagopoulos, Skyrmion qubits: A new class of quantum logic elements based on nanoscale magnetization, *Phys. Rev. Lett.* **127**, 067201 (2021).
- [31] J. Xia, X. Zhang, X. Liu, Y. Zhou, and M. Ezawa, Universal quantum computation based on nanoscale skyrmion helicity qubits in frustrated magnets, *Phys. Rev. Lett.* **130**, 106701 (2023).
- [32] J. Zou, S. Bosco, B. Pal, S. S. Parkin, J. Klinovaja, and D. Loss, Domain wall qubits on magnetic racetracks, arXiv preprint arXiv:2212.12019 (2022).
- [33] N. D. Mermin, The topological theory of defects in ordered media, *Rev. Mod. Phys.* **51**, 591 (1979).
- [34] E. A. Stepanov, C. Dutreix, and M. I. Katsnelson, Dynamical and reversible control of topological spin textures, *Phys. Rev. Lett.* **118**, 157201 (2017).
- [35] C. Chappert, A. Fert, and F. N. Van Dau, The emergence of spin electronics in data storage, *Nat. Mater.* **6**, 813 (2007).
- [36] M. Nakahara, *Geometry, topology and physics* (CRC press, 2018).
- [37] J. C. Baez and J. P. Muniain, *Gauge fields, knots and gravity*, Vol. 4 (World Scientific Publishing Company, 1994).
- [38] T. Frankel, *The geometry of physics: an introduction* (Cambridge university press, 2011).
- [39] D. Makarov and D. D. Sheka, *Curvilinear Micromagnetism: From Fundamentals to Applications*, Vol. 146 (Springer Nature, 2022).
- [40] D. Makarov, O. M. Volkov, A. Kákay, O. V. Pylypovskiy, B. Budinská, and O. V. Dobrovolskiy, New dimension in magnetism and superconductivity: 3d and curvilinear nanoarchitectures, *Adv. Mater.* **34**, 2101758 (2022).
- [41] R. Streubel, P. Fischer, F. Kronast, V. P. Kravchuk, D. D. Sheka, Y. Gaididei, O. G. Schmidt, and D. Makarov, Magnetism in curved geometries, *J. Phys. D: Appl. Phys.* **49**, 363001 (2016).
- [42] M.-C. Wang, C.-C. Huang, C.-H. Cheung, C.-Y. Chen, S. G. Tan, T.-W. Huang, Y. Zhao, Y. Zhao, G. Wu, Y.-P. Feng, H.-C. Wu, and C.-R. Chang, Prospects and opportunities of 2d van der waals magnetic systems, *Ann. Phys.* **532**, 1900452 (2020).
- [43] D. Sanz-Hernández, A. Hierro-Rodríguez, C. Donnelly, J. Pablo-Navarro, A. Sorrentino, E. Pereiro, C. Magén, S. McVitie, J. M. de Teresa, S. Ferrer, P. Fischer, and A. Fernández-Pacheco, Artificial double-helix for geometrical control of magnetic chirality, *ACS Nano* **14**, 8084 (2020).
- [44] D. D. Sheka, O. V. Pylypovskiy, O. M. Volkov, K. V. Yershov, V. P. Kravchuk, and D. Makarov, Fundamentals of curvilinear ferromagnetism: Statics and dynamics of geometrically curved wires and narrow ribbons, *Small* **18**, 2105219 (2022).
- [45] A. Fernández-Pacheco, R. Streubel, O. Fruchart, R. Hertel, P. Fischer, and R. P. Cowburn, Three-dimensional nanomagnetism, *Nat. Commun.* **8**, 15756 (2017).
- [46] C. Donnelly, A. Hierro-Rodríguez, C. Abert, K. Witte, L. Skoric, D. Sanz-Hernández, S. Finizio, F. Meng, S. McVitie, J. Raabe, D. Suess, R. Cowburn, and A. Fernández-Pacheco, Complex free-space magnetic field textures induced by three-dimensional magnetic nanostructures, *Nat. Nanotechnol.* **17**, 136 (2022).
- [47] C. Donnelly, M. Guizar-Sicairos, V. Scagnoli, S. Gliga, M. Holler, J. Raabe, and L. J. Heyderman, Three-dimensional magnetization structures revealed with x-ray vector nanotomography, *Nature* **547**, 328 (2017).
- [48] Y. Tserkovnyak, Perspective: (beyond) spin transport in insulators, *J. Appl. Phys.* **124**, 190901 (2018).
- [49] M. Tanhayi Ahari, S. Zhang, J. Zou, and Y. Tserkovnyak, Biasing topological charge injection in topological matter, *Phys. Rev. B* **104**, L201401 (2021).
- [50] J. Schwichtenberg, Demystifying gauge symmetry (2019), arXiv:1901.10420 [physics.hist-ph].
- [51] R. D. Kamien, The geometry of soft materials: a primer, *Rev. Mod. Phys.* **74**, 953 (2002).
- [52] A. Zee, *Quantum field theory in a nutshell* (2003).
- [53] S. G. Avery and B. U. W. Schwab, Noether's second theorem and ward identities for gauge symmetries, *J. High Energy Phys.* **2016** (2), 31.
- [54] J. A. Harvey, Magnetic monopoles, duality, and supersymmetry (1996), arXiv:hep-th/9603086 [hep-th].
- [55] V. Vitelli and A. M. Turner, Anomalous coupling between topological defects and curvature, *Phys. Rev. Lett.* **93**, 215301 (2004).
- [56] Y. Gaididei, V. P. Kravchuk, and D. D. Sheka, Curvature effects in thin magnetic shells, *Phys. Rev. Lett.* **112**, 257203 (2014).
- [57] J. M. Kosterlitz and D. J. Thouless, Ordering, metastability and phase transitions in two-dimensional systems, *J. Phys. C* **6**, 1181 (1973).
- [58] M. Stone and P. Goldbart, *Mathematics for Physics: A Guided Tour for Graduate Students* (Cambridge University Press, 2009).
- [59] See Supplemental Material at [] for (i) the construction of the gauge-invariant winding density, (ii) the differential geometric formulation of topological hydrodynamics, (iii) a derivation of the torsion of a uniform helix, and (iv) a discussion on how R_v , C_v , and \mathfrak{R} are estimated.
- [60] R. Naaman and D. H. Waldeck, Chiral-induced spin selectivity effect, *J. Phys. Chem. Lett.* **3**, 2178 (2012), pMID: 26295768.
- [61] S. Dalum and P. Hedegård, Theory of chiral induced spin selectivity, *Nano Lett.* **19**, 5253 (2019), pMID: 31265313.
- [62] R. Streubel, F. Kronast, P. Fischer, D. Parkinson, O. G. Schmidt, and D. Makarov, Retrieving spin textures on curved magnetic thin films with full-field soft x-ray microscopies, *Nat. Commun.* **6**, 7612 (2015).
- [63] L. Onsager, Reciprocal relations in irreversible processes. i., *Phys. Rev.* **37**, 405 (1931).
- [64] I. Gyarmati *et al.*, *Non-equilibrium thermodynamics*, Vol. 184 (Springer, 1970).
- [65] T. Yokouchi, F. Kagawa, M. Hirschberger, Y. Otani, N. Nagaosa, and Y. Tokura, Emergent electromagnetic induction in a helical-spin magnet, *Nature* **586**, 232 (2020).
- [66] E. Sonin, Spin currents and spin superfluidity, *Advances in Physics* **59**, 181 (2010).
- [67] S. K. Kim, S. Takei, and Y. Tserkovnyak, Thermally activated phase slips in superfluid spin transport in magnetic wires, *Phys. Rev. B* **93**, 020402 (2016).

- [68] A. Majumdar, Thermoelectricity in semiconductor nanostructures, *Science* **303**, 777 (2004).
- [69] A. A. Kovalev and Y. Tserkovnyak, Magnetocaloritronic nanomachines, *Solid State Commun.* **150**, 500 (2010), spin Caloritronics.
- [70] G. E. W. Bauer, S. Bretzel, A. Brataas, and Y. Tserkovnyak, Nanoscale magnetic heat pumps and engines, *Phys. Rev. B* **81**, 024427 (2010).
- [71] C. Phatak, Y. Liu, E. B. Gulsoy, D. Schmidt, E. Franke-Schubert, and A. Petford-Long, Visualization of the magnetic structure of sculpted three-dimensional cobalt nanospirals, *Nano Lett.* **14**, 759 (2014).
- [72] L. Skoric, D. Sanz-Hernández, F. Meng, C. Donnelly, S. Merino-Aceituno, and A. Fernández-Pacheco, Layer-by-layer growth of complex-shaped three-dimensional nanostructures with focused electron beams, *Nano Lett.* **20**, 184 (2020).

Supplemental Material for “Topological transport of vorticity on curved magnetic membranes”

Chau Dao,¹ Ji Zou,² Eric Kleinherbers,¹ and Yaroslav Tserkovnyak¹

¹*Department of Physics and Astronomy and Bhaumik Institute for Theoretical Physics,
University of California, Los Angeles, California 90095, USA*

²*Department of Physics, University of Basel, Klingelbergstrasse 82, CH-4056 Basel, Switzerland*

In this Supplemental Material, we provide (i) the construction of the gauge-invariant winding density, (ii) the differential geometric formulation of topological hydrodynamics, (iii) a derivation of the torsion of a uniform helix, and (iv) a discussion on how the vortex circuit elements R_v , C_v , and \mathfrak{R} are estimated.

(i) Gauge-invariant winding density

In this section, we construct the gauge-invariant winding density, discussed in the section “Gauge-invariant topological charge” of the main text. This winding density is the starting point for formulating topological hydrodynamics of vortices on curved magnetic membranes. Let us consider a curved dynamical two-dimensional magnetic membrane. The membrane is a two-dimensional orientable manifold \mathcal{M} with boundary $\partial\mathcal{M}$ and is parameterized by global coordinates ξ^1 and ξ^2 . \mathcal{M} is embedded in the Euclidean space \mathbb{R}^3 from which it inherits the metric g_{ij} . At every point (ξ^1, ξ^2) on \mathcal{M} and for any time t , we identify a unit normal vector $\mathbf{n}(t, \xi^1, \xi^2)$ and define unit vectors spanning the local tangent plane, $\mathbf{e}_1(t, \xi^1, \xi^2)$ and $\mathbf{e}_2(t, \xi^1, \xi^2)$. $\{\mathbf{e}_1, \mathbf{e}_2, \mathbf{n}\}$ form an orthonormal triad and is the local frame. We make the convention in which Greek indices $\mu = 0, 1, 2 \leftrightarrow t, \xi^1, \xi^2$ label spacetime coordinates, Latin indices $i = 1, 2 \leftrightarrow \xi^1, \xi^2$ label spatial coordinates, while repeated indices are summed over.

The magnetic texture is described by the continuum coarse-grained vector field $\mathbf{m}(\mathbf{r}, t)$. In the low-temperature ordered phase, \mathbf{m} exhibits only orientational dynamics and is normalized by its $T = 0$ value. On the other hand, in the high-temperature paramagnetic regime \mathbf{m} can fluctuate in both magnitude and direction. To construct the gauge-invariant winding density, it is useful to first specialize to the ordered phase and take the strong easy-surface limit, in which $|\mathbf{m}| = 1$ and \mathbf{m} lies fully within the local tangent plane. \mathbf{m} can be written in the local frame as

$$\mathbf{m}(t, \xi^1, \xi^2) = \mathbf{e}_1 \cos \varphi + \mathbf{e}_2 \sin \varphi, \quad (\text{S1})$$

where φ is the in-(tangent)-plane angle of \mathbf{m} relative to \mathbf{e}_1 . For a closed loop $\partial\mathcal{S}$ on \mathcal{M} , φ realizes the map $S^1 \mapsto S^1$. For flat manifolds, the winding number would simply be the degree of this map and would be given by $\mathcal{Q} = \int_{\partial\mathcal{S}} d\xi^i \mathbf{m}_i^2 \partial_i \varphi / 2\pi$ [1, 2]. However, different from winding in flat geometries, the local frame cannot be made constant, and will generally vary over \mathcal{M} . This means that $\partial_i \varphi$ would not be gauge-invariant. To define the winding, we must be able to compare the phase φ of the magnetization at different points on the curved manifold. Taking the derivative of \mathbf{m} and projecting onto the local basis vectors, we find that

$$\mathbf{e}_1 \cdot \partial_i \mathbf{m} = -\sin \varphi [\partial_i \varphi - \mathbf{e}_1 \cdot \partial_i \mathbf{e}_2], \quad (\text{S2a})$$

$$\mathbf{e}_2 \cdot \partial_i \mathbf{m} = \cos \varphi [\partial_i \varphi - \mathbf{e}_1 \cdot \partial_i \mathbf{e}_2]. \quad (\text{S2b})$$

Both expressions yield the same bracketed expression. The first term in the brackets is the winding of the in-plane angle and the second term is the the winding of the phase that is induced by curvature. Formally, the second term in the brackets is the connection on the manifold,

$$\mathcal{A}_i \equiv \mathbf{e}_1 \cdot \partial_i \mathbf{e}_2, \quad (\text{S3})$$

which captures the changes in \mathbf{e}_1 and \mathbf{e}_2 along ξ^i . If the manifold is dynamic, the local frame will be time-dependent and we can define $\mathcal{A}_0 = \mathbf{e}_1 \cdot \partial_t \mathbf{e}_2$, which tracks changes of the local frame in time. Together with the connection, we can define $\mathcal{A}_\mu = \mathbf{e}_1 \cdot \partial_\mu \mathbf{e}_2$ as the gauge potential which stems from the U(1) gauge freedom corresponding to rotations of \mathbf{e}_1 and \mathbf{e}_2 about \mathbf{n} . The term in the brackets of Eq. S2 is a gauge-invariant quantity, which we define as

$$D_i \varphi \equiv \partial_i \varphi - \mathcal{A}_i, \quad (\text{S4})$$

the *covariant change of the phase* φ , which is gauge-invariant. This construction of $D_i \varphi$ closely follows that done in Ref. [3]. Having constructed $D_i \varphi$, let us relax the constraint taken earlier, in which we specialized to the low-temperature ordered phase and took the strong-easy surface limit. We now allow \mathbf{m} to traverse out of the local tangent

plane and fluctuate in both magnitude and direction. For flat systems, it is known that the winding density along a curve parameterized is $\mathbf{m}_{\parallel}^2 \partial_{\ell} \varphi / 2\pi$ [1]. We can generalize this result for curved systems by making the substitution $\partial_i \varphi \rightarrow D_i \varphi$ so that the covariant winding is

$$d\xi^i \frac{1}{2\pi} \mathbf{m}_{\parallel}^2 D_i \varphi = d\xi^i \frac{1}{2\pi} \mathbf{m}_{\parallel}^2 (\partial_i \varphi - \mathcal{A}_i), \quad (\text{S5})$$

which is also gauge-invariant. The topological charge \mathcal{Q} enclosed on a patch \mathcal{S} of the manifold is consequently

$$\mathcal{Q} = \int_{\partial \mathcal{S}} \rho_w = \frac{1}{2\pi} \int_{\partial \mathcal{S}} d\xi^i \mathbf{m}_{\parallel}^2 D_i \varphi, \quad (\text{S6})$$

where ρ_w is the gauge-invariant winding 1-form. The relation between \mathcal{Q} and the winding density is given by Eq. (5) in the main text. Thus, we have constructed the winding density for a curved magnetic membrane and connected it to the gauge-invariant topological charge \mathcal{Q} .

It is advantageous to be able to write the winding density ρ_w in terms of \mathbf{m} rather than the in-plane angle φ . Doing so allows us to describe the topological charge density using a nonsingular vector field \mathbf{m} . On the other hand, the φ field is not defined at the center of the vortex. To this end, we define the covariant derivative of \mathbf{m} as

$$\nabla_{\mu} \mathbf{m} \equiv (\partial_{\mu} m^a) \mathbf{e}_a - \mathcal{A}_{\mu} \mathbf{n} \times \mathbf{m}. \quad (\text{S7})$$

This is identical to Eq. (4) of the main text. Here, $\mathcal{A}_{\mu} = \mathbf{e}_1 \cdot \partial_{\mu} \mathbf{e}_2$ can be understood as a gauge potential that tracks changes in the local frame in space as well as time. The covariant derivative acts on \mathbf{m} by first projecting out any components parallel to the normal vector \mathbf{n} , taking the derivative ∂_i , and then projecting the result back to the local tangent plane. Thus the covariant derivative of any vector in \mathbb{R}^3 will always result in a vector lying in the local tangent plane. Using this covariant derivative, we can express the winding 1-form in terms of \mathbf{m} as

$$\rho_w = d\xi^i \mathbf{n} \cdot (\mathbf{m} \times \nabla_i \mathbf{m}) / 2\pi, \quad (\text{S8})$$

which is the integrand of Eq. (13) in the main text. Finally, we elaborate on a point made in the last paragraph of the section ‘‘Gauge-invariant topological charge’’ regarding the quantization of \mathcal{Q} . Generally, when there is nonzero Gaussian curvature, even when taking the strong-easy surface limit, \mathcal{Q} is noninteger valued. A cartoon depiction of the vorticity density \mathcal{J}^0 for flat and curved membranes, with and without taking the easy-surface limit, is depicted in Fig. 1. Note that \mathcal{J}^0 is given by Eq. (3) of the main text.

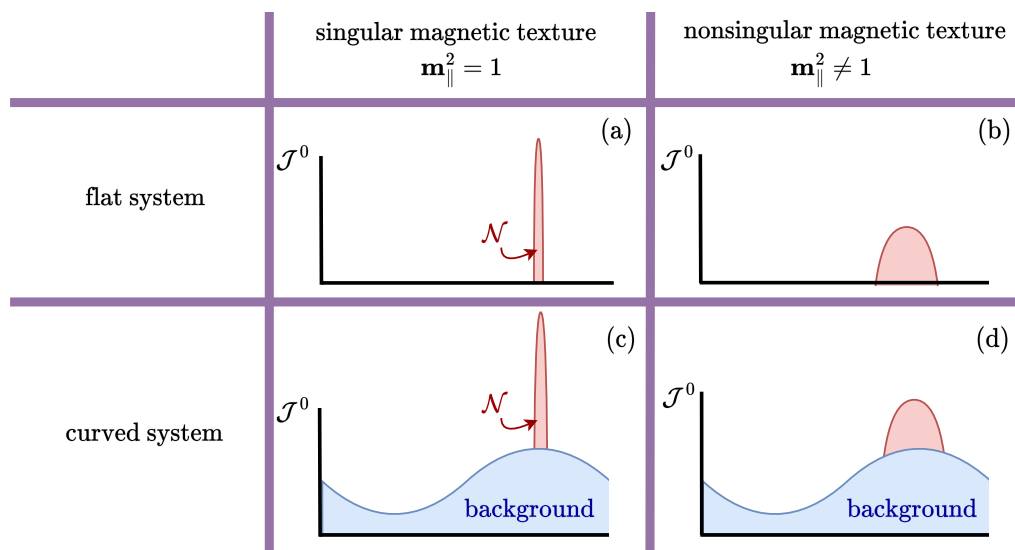


FIG. 1. Cartoon depiction of the vorticity density for flat and curved magnetic membranes, and for singular and nonsingular magnetic textures. Panel (a) shows that for a flat magnetic system, taking the strong easy-plane limit in which $\mathbf{m}_{\parallel}^2 = 1$ results in the magnetic texture becoming singular, and the vorticity density is a δ -function at the location of the vortex. Panel (b) shows that relaxing the strong easy-plane limit and allowing the magnetic texture to be nonsingular results in broadening of the delta function. Panels (c) and (d) shows that the effect of nonzero curvature is to add a background offset.

Taking the strong easy-surface limit, the topological charge on a patch \mathcal{S} (upon picking a smooth gauge) of the membrane can be evaluated as

$$\mathcal{Q} = \mathcal{N} - \frac{1}{2\pi} \int_{\mathcal{S}} d\xi^1 d\xi^2 \sqrt{g} \mathcal{K}, \quad (\text{S9})$$

where \mathcal{K} is the local Gaussian curvature and g is the determinant of the metric. The topological charge is the difference of an integer \mathcal{N} , which counts the number of vortices on \mathcal{S} , and a geometrical background offset that spoils the discreteness of \mathcal{Q} . The effect of this background offset is depicted in panels (c) and (d) of Fig. 1. When the strong-easy surface limit is taken, we find that the vorticity density sharply peaks at the location of the vortex. In the extreme case, when $|\mathbf{m}_{\parallel}| = 1$ everywhere except for the location of the vortex, at which there is a singularity in the \mathbf{m} vector field, \mathcal{J}^0 is proportional to the δ -function. However, by relaxing the strong easy-surface limit, we allow for a nonsingular magnetic texture and the vorticity density is no longer a δ -function. In this case, the δ -function broadens, as shown in panels (b) and (d).

(ii) Formulation of topological hydrodynamics

In this section, we start from the covariant winding density and construct the vorticity 3-current, \mathcal{J}^μ . We first specialize to the static manifold, in which the local frame has no time dependence. We will show that \mathcal{J}^μ satisfies the topological continuity equation $\partial_\mu \mathcal{J}^\mu = 0$, even when \mathbf{m} can fluctuate. Furthermore, we demonstrate that the continuity equation is still satisfied when the membrane is dynamic and the time dependence of the local frame is restored. To do so, we will formulate topological hydrodynamics using differential forms, as discussed in the ‘‘Discussion’’ section of the main text. The topological charge on a patch \mathcal{S} of the manifold \mathcal{M} is

$$\mathcal{Q} = \int_{\partial\mathcal{S}} \rho_w = \frac{1}{2\pi} \int_{\partial\mathcal{S}} d\xi^i \mathbf{n} \cdot (\mathbf{m} \times \nabla_i \mathbf{m}), \quad (\text{S10})$$

which is defined as the integral of the winding 1-form ρ_w over the boundary of the patch, $\partial\mathcal{S}$. After defining the winding 1-form, we invoke the generalized Stoke’s theorem to define the vorticity 2-form as the exterior derivative of ρ_w . We have that

$$\begin{aligned} \rho_v \equiv d\rho_w &= d\xi^i \wedge d\xi^j \frac{1}{2\pi} \mathbf{n} \cdot \left(\nabla_i \mathbf{m} \times \nabla_j \mathbf{m} + \frac{\mathbf{m} \times [\nabla_i, \nabla_j] \mathbf{m}}{2} \right) \\ &= d\xi^i \wedge d\xi^j \frac{1}{2\pi} \mathbf{n} \cdot \left(\nabla_i \mathbf{m} \times \nabla_j \mathbf{m} - \frac{1}{2} \mathcal{F}_{ij} \mathbf{m}_{\parallel}^2 \right). \end{aligned} \quad (\text{S11})$$

Here, $d \equiv d\xi^i \wedge \partial_i$ is the exterior derivative and $\mathcal{F}_{ij} = \partial_i \mathcal{A}_j - \partial_j \mathcal{A}_i$ is the gauge-invariant curvature field which arises from the connection \mathcal{A}_i on \mathcal{M} . The curvature field \mathcal{F}_{ij} is related to the Gaussian curvature \mathcal{K} by $\mathcal{K} = \epsilon^{0ij} \mathcal{F}_{ij} / 2\sqrt{g}$. Here, we use the Levi-Civita convention that $\epsilon^{012} = 1$. Furthermore, \mathcal{F}_{ij} is the ‘‘magnetic’’ component of the field strength tensor $\mathcal{F}_{\mu\nu}$ given by Eq. (2) of the main text. The scalar vorticity density on the manifold is the Hodge dual of the vorticity 2-form and is written as

$$\star\rho_v = \frac{\epsilon^{0ij}}{2\pi\sqrt{g}} \mathbf{n} \cdot \left(\nabla_i \mathbf{m} \times \nabla_j \mathbf{m} - \frac{1}{2} \mathcal{F}_{ij} \mathbf{m}_{\parallel}^2 \right). \quad (\text{S12})$$

In this expression, we have used the Hodge star map ‘‘ \star ’’, which maps a p -form in d -dimensional space to its Hodge dual, a $(d-p)$ -form. The mapping is defined to be [4]

$$\star d\xi^{i_1} \dots d\xi^{i_p} = \frac{1}{(d-p)!} \sqrt{g} g^{i_1 j_1} \dots g^{i_p j_p} \epsilon_{j_1 \dots j_p j_{p+1} \dots j_d} d\xi^{j_{p+1}} \dots d\xi^{j_d}. \quad (\text{S13})$$

For any change of the charge \mathcal{Q} on \mathcal{S} , we expect to find a vorticity flux j_v through the boundary $\partial\mathcal{S}$, which changes the winding along the boundary. That is, we wish to find a j_v that satisfies the continuity equation

$$\star\partial_t \rho_v + \star d \star j_v = 0. \quad (\text{S14})$$

The first term in Eq. (S14), $\star\partial_t \rho_v$, is the time derivative of the vorticity density, and the second term $\star d \star j_v$ is the divergence of the vorticity flux. To construct j_v , we return to the generalized Stokes’ theorem, which states that $\rho_v = d\rho_w$. Taking the time derivative and applying the Hodge star operator to both sides of this expression, we get

$$\star\partial_t \rho_v - \star\partial_t d\rho_w = 0 \quad (\text{S15})$$

Using the property of the Hodge star that for any p -form ω , applying the Hodge star map twice yields $\star\star\omega = (-1)^{d-p}\omega$, we can rewrite Stokes' theorem as

$$\partial_t(\star\rho_v) + \star d\star(\star\partial_t\rho_w) = 0. \quad (\text{S16})$$

We identify the vorticity flux j_v with $\star\partial_t\rho_w$, and so

$$\begin{aligned} j_v &= \frac{1}{\pi} \star [d\xi^i \mathbf{n} \cdot (\partial_t \mathbf{m} \times \nabla_i \mathbf{m})] \\ &= d\xi^k \frac{1}{\pi} \mathbf{n} \cdot (\partial_t \mathbf{m} \times \nabla_i \mathbf{m}) \sqrt{g} g^{ij} \epsilon_{jk}, \end{aligned} \quad (\text{S17})$$

with the vector components of the vorticity flux given by

$$j_v^i = \frac{1}{\sqrt{g}\pi} \mathbf{n} \cdot (\partial_t \mathbf{m} \times \nabla_j \mathbf{m}) \epsilon^{ji}. \quad (\text{S18})$$

The topological continuity equation is simply a reformulation of the generalized Stokes' theorem. Importantly, in deriving this continuity equation we have not specified any Lagrangian. Therefore, this continuity equation and conservation of the vorticity density is robust and will not be spoiled by any disorder or structural symmetries associated with the Lagrangian.

The scalar vorticity density and the vectorial vorticity flux can be combined into a vorticity 3-current $\mathcal{J}^\mu = (\mathcal{J}^0, \mathcal{J})$, where \mathcal{J}^0 is understood as the vorticity density and \mathcal{J} is the vorticity flux. Using Eqs. (S12) and (S17), we see that \mathcal{J}^μ is given by

$$\mathcal{J}^\mu = \frac{\epsilon^{\mu\nu\rho}}{2\pi} \left[\mathbf{n} \cdot (\nabla_\nu \mathbf{m} \times \nabla_\rho \mathbf{m}) - \frac{1}{2} \mathcal{F}_{\nu\rho} \mathbf{m}_\parallel^2 \right]. \quad (\text{S19})$$

This expression for the vorticity 3-current is given by Eq. (3) in the main text. Here, $\mathcal{F}_{\nu\rho}$ can be understood as the gauge-invariant field strength tensor, analogous to \mathcal{A}_μ being understood as the gauge potential. The ‘‘magnetic’’ component of the field strength tensor is the curvature field \mathcal{F}_{ij} .

We can directly check that the continuity $\partial_\mu \mathcal{J}^\mu = 0$ is satisfied for \mathcal{J}^μ in Eq. (S19). Let us now allow the membrane to be dynamic and demonstrate that the continuity equation is still satisfied even when the membrane can fluctuate. Doing so, the ‘‘electric’’ component of the field strength tensor is now nonzero, and \mathbf{e}_1 , \mathbf{e}_2 , and \mathbf{n} may be time dependent. \mathbf{m} may also fluctuate in both orientation as well as magnitude. We have that

$$\partial_\mu \mathcal{J}^\mu = \partial_\mu \left\{ \frac{\epsilon^{\mu\nu\rho}}{2\pi} \left[\mathbf{n} \cdot (\nabla_\nu \mathbf{m} \times \nabla_\rho \mathbf{m}) - \frac{1}{2} \mathcal{F}_{\nu\rho} \mathbf{m}_\parallel^2 \right] \right\} \quad (\text{S20})$$

Let us simplify the first and second terms in the brackets separately by expanding the covariant derivative and expressing the terms with the regular derivative ∂_μ and the gauge potential \mathcal{A}_μ . For the first term, we have

$$\begin{aligned} \frac{\epsilon^{\mu\nu\rho}}{2\pi} [\mathbf{n} \cdot (\nabla_\nu \mathbf{m} \times \nabla_\rho \mathbf{m})] &= \frac{\epsilon^{\mu\nu\rho}}{2\pi} \{ (\partial_\nu m^a) (\partial_\rho m^b) \mathbf{n} \cdot (\mathbf{e}_a \times \mathbf{e}_b) - \mathcal{A}_\rho (\partial_\nu m^a) m^b \mathbf{n} \cdot [\mathbf{e}_a \times (\mathbf{n} \times \mathbf{e}_b)] \\ &\quad - \mathcal{A}_\nu (\partial_\rho m^b) m^a \mathbf{n} \cdot [(\mathbf{n} \times \mathbf{e}_a) \times \mathbf{e}_b] \} \\ &= \frac{\epsilon^{\mu\nu\rho}}{2\pi} \{ (\partial_\nu m^a) (\partial_\rho m^b) \mathbf{n} \cdot (\mathbf{e}_a \times \mathbf{e}_b) - 2\mathcal{A}_\rho (\partial_\nu m^a) m^b \mathbf{n} \cdot [\mathbf{e}_a \times (\mathbf{n} \times \mathbf{e}_b)] \} \\ &= \frac{\epsilon^{\mu\nu\rho}}{2\pi} \{ (\partial_\nu m^a) (\partial_\rho m^b) \mathbf{n} \cdot (\mathbf{e}_a \times \mathbf{e}_b) - \mathcal{A}_\rho \partial_\nu (\mathbf{m}_\parallel^2) \} \end{aligned} \quad (\text{S21})$$

Taking the divergence of the simplified first term, we see that

$$\frac{\epsilon^{\mu\nu\rho}}{2\pi} \partial_\mu [\mathbf{n} \cdot (\nabla_\nu \mathbf{m} \times \nabla_\rho \mathbf{m})] = -\frac{\epsilon^{\mu\nu\rho}}{2\pi} (\partial_\mu \mathcal{A}_\rho) \partial_\nu (\mathbf{m}_\parallel^2) = \frac{\epsilon^{\mu\nu\rho}}{2\pi} \frac{\mathcal{F}_{\nu\rho}}{2} \partial_\mu (\mathbf{m}_\parallel^2). \quad (\text{S22})$$

Here, we have used the fact that the contraction of the antisymmetric Levi-Civita symbol $\epsilon^{\mu\nu\rho}$ with the symmetric terms $\partial_\mu \partial_\nu m^a$ and $\partial_\mu \partial_\rho m^b$ is zero. We also use the fact that $\mathbf{n} \cdot (\mathbf{e}_a \times \mathbf{e}_b)$ is a constant. Next, we take the divergence of the second term to get

$$\frac{\epsilon^{\mu\nu\rho}}{2\pi} \partial_\mu \left(-\frac{1}{2} \mathcal{F}_{\nu\rho} \mathbf{m}_\parallel^2 \right) = -\frac{\epsilon^{\mu\nu\rho}}{2\pi} \frac{\mathcal{F}_{\nu\rho}}{2} \partial_\mu (\mathbf{m}_\parallel^2), \quad (\text{S23})$$

using the identity that $\epsilon^{\mu\nu\rho} \partial_\mu \mathcal{F}_{\nu\rho} = 0$. Since the two terms sum to zero, it is indeed true that

$$\partial_\mu \mathcal{J}^\mu = 0. \quad (\text{S24})$$

(iii) Torsion of a curve/helix

Torsion is a geometric property of a curve embedded in \mathbb{R}^3 which can be used to reduce symmetries and enable vortex dynamics. In this section, we will calculate the torsion of a uniform helix, which is used in the setup discussed in the main text. A uniform helix can generally be described by

$$\mathbf{r}(\ell) = \left(r \cos \frac{\omega \ell}{c}, r \sin \frac{\omega \ell}{c}, \frac{b}{c} \ell \right). \quad (\text{S25})$$

Let us assume $r, \omega, c > 0$, and then the sign of b determines the chirality of the helix. $\text{sgn}(b) = \pm 1$ corresponds to positive or negative chirality. The velocity is given by:

$$\mathbf{v} = \frac{d\mathbf{r}}{d\ell} = \left(-\frac{r\omega}{c} \sin \frac{\omega \ell}{c}, \frac{r\omega}{c} \cos \frac{\omega \ell}{c}, \frac{b}{c} \right), \quad (\text{S26})$$

which is not unity. Imposing the constraint that $|\mathbf{v}| = 1$, we obtain $c^2 = r^2\omega^2 + b^2$. Therefore, we should take $c = \sqrt{r^2\omega^2 + b^2}$ when using the arc length to parameterize the helix. The acceleration is given by

$$\frac{d\mathbf{v}}{d\ell} = \left(-\frac{r\omega^2}{c^2} \cos \frac{\omega \ell}{c}, -\frac{r\omega^2}{c^2} \sin \frac{\omega \ell}{c}, 0 \right). \quad (\text{S27})$$

The curvature is its magnitude,

$$\kappa(\ell) = \frac{r\omega^2}{c^2}, \quad (\text{S28})$$

which is independent of ℓ . The normal vector is then

$$\mathbf{a}(\ell) = \frac{d\mathbf{v}/d\ell}{\kappa} = \left(-\cos \frac{\omega \ell}{c}, -\sin \frac{\omega \ell}{c}, 0 \right). \quad (\text{S29})$$

We can then determine the bi-normal vector

$$\mathbf{b}(\ell) = \mathbf{v} \times \mathbf{a} = \left(\frac{b}{c} \sin \frac{\omega \ell}{c}, -\frac{b}{c} \cos \frac{\omega \ell}{c}, \frac{r\omega}{c} \right). \quad (\text{S30})$$

To determine the torsion, we evaluate the changing rate of this vector, which yields

$$\frac{d\mathbf{b}}{d\ell} = \left(\frac{b\omega}{c^2} \cos \frac{\omega \ell}{c}, \frac{b\omega}{c^2} \sin \frac{\omega \ell}{c}, 0 \right). \quad (\text{S31})$$

We recall the definition of the torsion, $\frac{d\mathbf{b}}{d\ell} = -\mathfrak{T}\mathbf{a}$, from which we obtain the torsion

$$\mathfrak{T}(\ell) = \frac{b\omega}{c^2} = \frac{b\omega}{r^2\omega^2 + b^2}. \quad (\text{S32})$$

We remark that both curvature and torsion of a helix are independent of the point ℓ , as one may expect. It is important to notice that the torsion changes the sign when we switch the chirality of the helix. Finally, the torsion can be written in terms of the helix angle θ . To see this, we first note that

$$\sin \theta = \frac{b}{\sqrt{r^2\omega^2 + b^2}}, \quad \cos \theta = \frac{r\omega}{\sqrt{r^2\omega^2 + b^2}} \quad (\text{S33})$$

The torsion can thus be written as

$$\mathfrak{T} = \frac{\sin(2\theta)}{2r}. \quad (\text{S34})$$

(iv) Estimation of effective vortex circuit elements

The section ‘‘Vortex circuit elements’’ in the main text introduces the effective vortex resistance R_v , the effective winding capacitance C_v , and the effective drag \mathfrak{R} for the setup of the cylindrical magnetic membrane wrapped with a wire. These circuit elements are then used to construct effective topological circuits. In this section, we elucidate how expressions for \mathfrak{R} , R_v and C_v may be estimated. First, let us describe the setup. A magnetic insulating membrane of thickness h and length l_m wraps around a cylindrical insulating core. A metal wire of width w and thickness δ is wrapped around the cylindrical magnetic membrane of radius r as a uniform helix with helix angle θ .

Although the magnetic membrane is curved, to estimate the vortex circuit elements, it is useful to ‘‘unroll’’ the cylinder and consider vortex dynamics on a flat magnetic membrane. This is depicted in Fig. 2. Here, we see that the magnetic membrane translates to a rectangle of width $2\pi r$ and length l_m . The helically wrapped wire translates into metallic stripes across the magnetic rectangle at angle θ and spaced out at distances of $2\pi r / \tan \theta$, which is the pitch of the helix. When an electric current flow is induced in the metallic wire, the electric current exerts a torque on the magnetic texture which acts to bias vorticity injection transverse to the wire. The magnetic system responds by exhibiting a vortex resistance, which can stem from Gilbert damping, vortex-antivortex collisions, and defects, and a winding capacitance, which arises due to the magnetic stiffness. The system depicted in Fig. (2) shows that the setup of the magnetic cylinder wrapped with a wire is effectively a series RC circuit of N batteries, a vortex resistor, and a winding capacitor, where

$$N = \frac{l_m \tan \theta}{2\pi r} \quad (\text{S35})$$

is the number of metallic stripes. Let us first derive the effective drag coefficient \mathfrak{R} . When electric current flow is induced in the metal wire, each metal stripe acts as a battery and supplies a vortex motive force

$$\Delta\mu = \zeta \mathfrak{T} j \quad (\text{S36})$$

to the effective vortex circuit. Here, ζ is the phenomenological parameter characterizing the charge-vortex coupling, \mathfrak{R} is the torsion, and j is the electric current density. The vortex chemical potential is taken from Eq. (7) in the main text. The total supplied motive force is thus

$$\mathcal{V} = N \Delta\mu = \frac{\zeta \mathfrak{T} l_m \tan \theta}{2\pi r} j = \frac{\zeta \mathfrak{T} l_m}{w \delta 2\pi r} I \tan \theta, \quad (\text{S37})$$

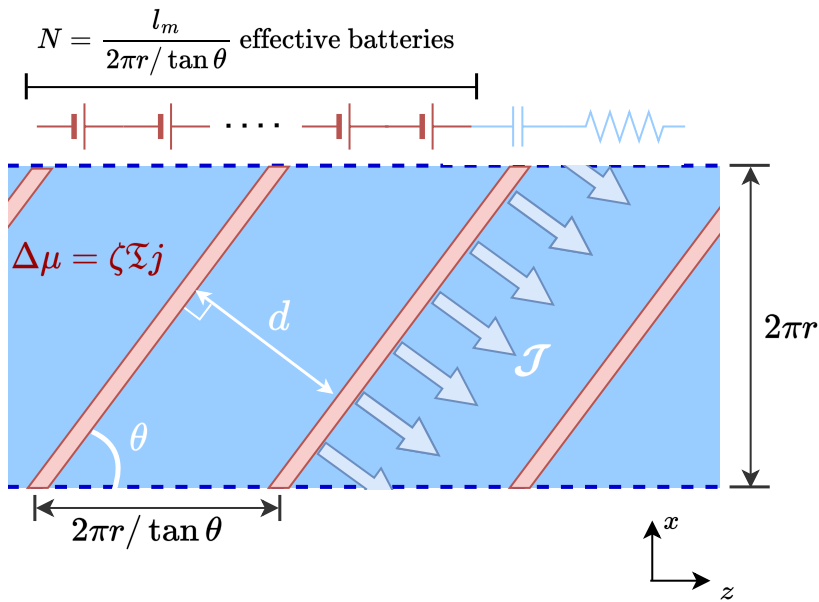


FIG. 2. An ‘‘unrolled’’ depiction of a cylindrical magnetic membrane. A metal wire is wrapped as a uniform helix around the magnetic cylinder. The wire translates into evenly spaced metal stripes in the flat depiction. The setup can be understood as a series $R_v C_v$ circuit of N batteries connected in series with the vortex resistance R_v and the winding capacitance C_v . Each battery which supplies a motive force $\Delta\mu$ to the effective vortex circuit when an electric current flow is induced in the wire.

where I is the electric current. The vortex motive force can be thought of as the drag force exerted by the electric current on vortices, where the drag coefficient is

$$\mathfrak{R} \equiv \frac{\mathcal{V}}{I} = \frac{\zeta \mathfrak{T} l_m}{w \delta 2\pi r} \tan \theta. \quad (\text{S38})$$

This is the same as Eq. (8) in the main text. Next, the vortex resistance can be estimated using Ohm's law. The component vortex flux \mathcal{J} which flows along the z direction is related to the supplied motive force by

$$\mathcal{J} \sin \theta = \sigma_v \frac{\mathcal{V}}{l_m}, \quad (\text{S39})$$

where σ_v is the vortex conductivity. The vortex current I_v which flows along z and builds up winding azimuthally is

$$I_v = 2\pi r \mathcal{J} \sin \theta. \quad (\text{S40})$$

Thus, we define the vortex resistance as

$$R_v \equiv \frac{\mathcal{V}}{I_v} = \frac{1}{\sigma_v} \frac{l_m}{2\pi r}. \quad (\text{S41})$$

Finally, we estimate the winding capacitance C_v . We assume that in the steady state, the magnetic texture is loaded with vortex charge \mathcal{Q}_s , and the azimuthal winding is homogenous, such that the winding density along a loop around the cylinder at fixed z is constant and may be given by

$$\frac{1}{2\pi} \mathbf{m}_{\parallel}^2 D_{\ell} \varphi = \frac{\mathcal{Q}_s}{2\pi r}. \quad (\text{S42})$$

Anticipating that the energy stored on the magnetic texture will be related to C_v by $\mathcal{E} = \mathcal{Q}_s^2/2C_v$, we can roughly estimate the steady-state energy that arises due to the magnetic winding by

$$\begin{aligned} \mathcal{E} &\sim \frac{hA}{2} \int dS (\mathbf{m}_{\parallel}^2 D_{\ell} \varphi)^2 \\ &= \frac{hA}{2} \int dS \left(\frac{\mathcal{Q}_s}{r} \right)^2 \\ &= \pi hA \mathcal{Q}_s^2 l_m / r \end{aligned} \quad (\text{S43})$$

Equating this with $\mathcal{Q}_s^2/2C_v$, we find that the winding capacitance may be estimated as

$$C_v = \frac{1}{A} \frac{r}{2\pi h l_m}. \quad (\text{S44})$$

-
- [1] J. Zou, S. K. Kim, and Y. Tserkovnyak, Topological transport of vorticity in heisenberg magnets, *Phys. Rev. B* **99**, 180402(R) (2019).
- [2] D. Jones, J. Zou, S. Zhang, and Y. Tserkovnyak, Energy storage in magnetic textures driven by vorticity flow, *Phys. Rev. B* **102**, 140411 (2020).
- [3] R. D. Kamien, The geometry of soft materials: a primer, *Rev. Mod. Phys.* **74**, 953 (2002).
- [4] M. Stone and P. Goldbart, *Mathematics for Physics: A Guided Tour for Graduate Students* (Cambridge University Press, 2009).